

INTERACTION BETWEEN INTERNAL NATURAL CONVECTION IN AN ENCLOSURE AND AN EXTERNAL NATURAL CONVECTION BOUNDARY-LAYER FLOW

E. M. SPARROW and C. PRAKASH

Department of Mechanical Engineering, University of Minnesota,
 Minneapolis, MN 55455, U.S.A.

(Received 10 September 1980 and in revised form 13 November 1980)

Abstract—An analysis is made of natural convection in a square enclosure, of which one vertical wall is cooled by an external natural convection boundary-layer flow. The other vertical wall is maintained at a uniform temperature while the horizontal walls are adiabatic. The resulting conjugate internal-external natural-convection problem was solved numerically for Grashof numbers between 10^3 and 10^7 and for a Prandtl number of 0.7. Approximate solutions were also obtained using a model which avoids conjugate-type computations. For comparison purposes, a set of solutions were carried out for the standard natural-convection enclosure problem characterized by prescribed uniform temperatures on the vertical walls and adiabatic horizontal walls. For the overall heat transfer characteristics encompassing both the internal and external flows, the average Nusselt number displayed a power-law dependence on the Grashof number given by $\overline{Nu} = 0.0907 Gr^{0.285}$ for $Gr \geq 10^4$. These Nusselt numbers are about sixty per cent of those for the standard enclosure, at common values of the respective Grashof numbers. The local heat flux variations along the convectively cooled wall were found to be appreciably smaller than those along the heated isothermal wall, reflecting the counterflow nature of the heat exchange between the internal and external flows. In addition, the temperature variations along the convectively cooled wall increased with increasing Grashof number. The Grashof number also decisively affected the temperature distributions along the adiabatic walls. Streamline maps revealed little difference between the flow fields adjacent to the thermally active and thermally passive walls at low Grashof numbers, but marked differences were in evidence at high Grashof numbers. For the external natural convection, the local heat transfer coefficients were generally larger than those predicted by the local application of the classical isothermal-plate heat transfer coefficient formula.

NOMENCLATURE

<p>Gr, Grashof number, equations (5) and (27);</p> <p>g, acceleration of gravity;</p> <p>h, local heat transfer coefficient for external flow;</p> <p>k, thermal conductivity;</p> <p>L, length of side of enclosure;</p> <p>\overline{Nu}, average Nusselt number, equations (25) and (27);</p> <p>P, dimensionless pressure, equation (4);</p> <p>Pr, Prandtl number;</p> <p>p, pressure;</p> <p>Q, overall rate of heat transfer;</p> <p>q, local heat flux;</p> <p>T, temperature;</p> <p>T_c, temperature of cooled wall for standard enclosure;</p> <p>T_h, temperature of isothermal heated wall;</p> <p>T_{wx}, temperature distribution along adiabatic walls;</p> <p>T_{wy}, temperature distribution along convectively cooled wall;</p> <p>T_∞, ambient temperature;</p> <p>u, v, velocity components;</p> <p>U, V, dimensionless velocities, equation (3);</p> <p>\hat{U}, \hat{V}, dimensionless velocities, equation (10);</p> <p>X, Y, dimensionless coordinates, equation (4);</p> <p>x, y, coordinates;</p> <p>x', coordinate, $(x - L)$;</p>	<p>β, coefficient of thermal expansion;</p> <p>θ, dimensionless temperature, $(T - T_\infty)/(T_h - T_\infty)$;</p> <p>$\nu$, kinematic viscosity;</p> <p>ρ, density;</p> <p>χ, dimensionless coordinate, equation (11);</p> <p>ψ, stream function;</p> <p>Ω, multiplying factor in representation of h, equations (22) and (30).</p>
--	---

INTRODUCTION

NATURAL convection within rectangular enclosures has attracted considerable attention in recent years both from an applications standpoint and as a standard problem for numerical computation. The standard problem is concerned with two-dimensional buoyancy-driven flow in a rectangle whose vertical sides are maintained at uniform but different temperatures while the horizontal sides are adiabatic. This situation is shown schematically in Fig. 1(a), where T_h and T_c denote the uniform temperatures of the vertical walls ($T_h > T_c$). There is extensive literature devoted to this problem, the earlier contributions to which were reviewed by Ostrach [1]. Representative contributions to the recent literature are typified by Jones [2] and Reddy and Satake [3]. These, together with the recently-published survey by Bejan [4], convey bibliographies encompassing the

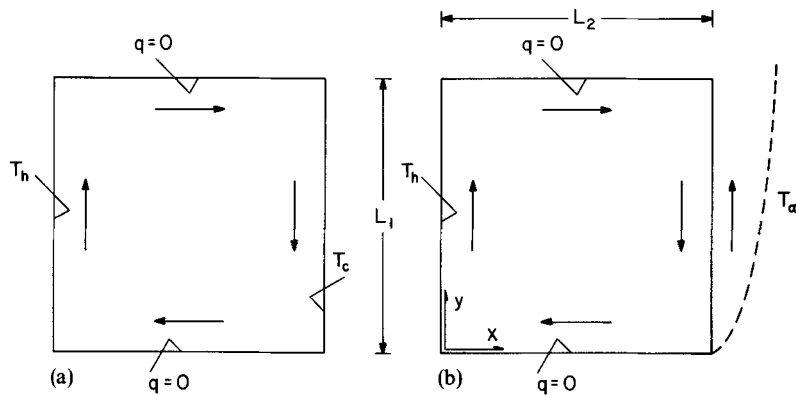


FIG. 1. Natural convection enclosure problems. (a) Standard enclosure problem with prescribed uniform temperatures on the vertical walls. (b) Conjugate internal buoyancy-driven flow and external natural convection boundary layer flow.

main work of the past decade.

Whereas the thermal boundary conditions indicated in Fig. 1(a) constitute a well-defined standard case, they are somewhat restrictive in that they do not reflect possible thermal interactions between the enclosure and the surroundings. Typical among such interactions would be the transfer of heat by natural convection between one of the walls of the enclosure and the adjacent surroundings. Such a situation is pictured schematically in Fig. 1(b), and this defines the problem that is the focus of the present study.

Examination of Fig. 1(a,b) reveals significant differences between the standard enclosure problem and that which is investigated here. The standard problem deals with the buoyancy-driven recirculating flow in the enclosure; it involves thermal boundary conditions on the enclosure walls which are known and specified in advance. However, the present problem actually deals with two flows—the recirculating flow in the enclosure and the external boundary layer flow along the right-hand wall of the enclosure. The temperatures T_h ($=$ constant) and T_∞ , respectively at the left-hand wall and in the ambient fluid, are regarded as being given; the temperature at the right-hand wall is unknown. Its magnitude and distribution along the height of the wall are determined by the dynamics of the heat transfer process. Thus, the full complement of thermal boundary conditions needed to solve either of the flows is not known in advance. Consequently, the solution scheme must accommodate thermal interactions between the internal and external flows such that the wall-temperature distribution emerges as one of the results.

Thus, the coupling of the two flows and the determination of the boundary conditions are distinguishing features of the present problem. In view of the coupling, the problem is of the conjugate type, and it is one of the few conjugate problems in the literature where the two contributing sub-problems

are both natural-convection flows.

The two natural-convection flows are, however, fundamentally different in nature. The external flow is a boundary layer. An essential feature of a boundary-layer flow is that the velocity and temperature at a given point are not influenced by happenings downstream of that point. Thus, a numerical solution can be obtained by a marching procedure which starts at the leading edge and proceeds downstream in the flow direction. On the other hand, because of the recirculating nature of the flow within the enclosure, the velocity and temperature at a point are influenced by both upstream and downstream happenings (indeed, that which is downstream of a point is also upstream). Thus, due to this coupling, a numerical solution for the fluid flow and temperature fields within the enclosure must deal simultaneously with all points.

Frequently, boundary layer and recirculating flow problems are respectively characterized as parabolic and elliptic—these designations coming from the mathematical and computational nature of the respective problems (marching vs all-point interaction). The need to deal with interacting parabolic and elliptic problems is another special feature of this study.

The flow directions indicated in Fig. 1(b) correspond to the condition $T_h > T_\infty$. The upflow in the external boundary layer and the downflow in the adjacent internal flow give rise to a counterflow heat exchange situation, the ramifications of which will be amplified during the presentation of results.

The solutions were carried out numerically for Grashof numbers $Gr = 10^3, 10^4, 10^5, 10^6$ and 10^7 . Not only were solutions obtained for the conjugate internal flow-external flow problem, but a set of solutions was also carried out for the standard enclosure problem (Fig. 1(a)). These supplementary solutions were obtained in order to provide perspective for the results of the conjugate problem. Although literature

solutions do exist for the standard problem, it was felt that for definitive comparisons of the standard and conjugate problems, both sets of solutions should be obtained with the same methodology and computational procedures.

For the solutions, the fluids within and external to the enclosure were assumed to have the same thermophysical properties, with Prandtl number $Pr = 0.7$. The enclosure was taken to be a square, such that $L_1 = L_2 = L$.

Results in dimensionless form will be presented for the overall rate of heat transfer across the enclosure and for the local rates of heat transfer at the thermally active walls. Temperature distributions for the right-hand wall will be reported, as will the temperature distributions along the two adiabatic walls. Flow patterns will be displayed in terms of streamline maps. Wherever appropriate, comparisons will be made between the results of the conjugate problem and those of the standard enclosure. In addition, results of a simplified computational model for the conjugate problem will also be presented in order to establish its accuracy.

ANALYSIS

Problem formulation

In formulating the conjugate internal flow-external flow natural convection problem, it is convenient first to deal serially with the conservation equations for each of the component problems. The formulation is then completed by the statement of the boundary conditions and of the matching conditions at the interface between the external and internal flows.

Attention is first directed at internal flow. The buoyancy force is deduced by considering the terms $(-\partial p/\partial y - \rho g)$ which appear in the y -momentum equation and then adding and subtracting the constant $\rho_\infty g$ (ρ_∞ corresponds to the density of the ambient fluid). When a Boussinesq-type equation of state, i.e.

$$\rho_\infty - \rho = \beta\rho(T - T_\infty) \quad (1)$$

is used, the foregoing terms become

$$-\partial(p + \rho_\infty g y)/\partial y + g\beta\rho(T - T_\infty). \quad (2)$$

The last term in equation (2) is readily identified with the buoyancy force while the quantity $(p + \rho_\infty g y)$ that appears in the first term is a hydrostatic-supplemented pressure. Note that the involvement of ρ_∞ as a datum is somewhat arbitrary. The density ρ_h associated with T_h could also have been used as the datum. In either case, the final dimensionless conservation equations are the same.

The dimensionless variables, coordinates and parameters which yield the simplest form of the conservation equations for the internal flow are

$$U = u/(v/L), \quad V = v/(v/L), \\ \theta = (T - T_\infty)/(T_h - T_\infty) \quad (3)$$

$$P = (p + \rho_\infty g y)/\rho(v/L)^2, \quad X = x/L, \quad Y = y/L \quad (4)$$

$$Gr = g\beta(T_h - T_\infty)L^3/v^2, \quad Pr = c_p\mu/k. \quad (5)$$

The conservation equations which result from the use of equations (2) through (5) are

$$\frac{\partial U}{\partial X} + \frac{\partial V}{\partial Y} = 0 \quad (6)$$

$$U \frac{\partial U}{\partial X} + V \frac{\partial U}{\partial Y} = -\frac{\partial P}{\partial X} + \nabla^2 U \quad (7)$$

$$U \frac{\partial V}{\partial X} + V \frac{\partial V}{\partial Y} = -\frac{\partial P}{\partial Y} + Gr\theta + \nabla^2 V \quad (8)$$

$$U \frac{\partial \theta}{\partial X} + V \frac{\partial \theta}{\partial Y} = \frac{1}{Pr} \nabla^2 \theta \quad (9)$$

in which $\nabla^2 = \partial^2/\partial X^2 + \partial^2/\partial Y^2$. These equations contain two dimensionless parameters, Gr and Pr .

Attention may now be turned to the external flow, which is a boundary-layer flow. Here, the buoyancy-related terms $(-\partial p/\partial y - \rho g)$ in the y -momentum equation become $(\rho_\infty g - \rho g)$ because $\partial p/\partial y = \partial p_\infty/\partial y = -\rho_\infty g$, and the density difference $(\rho_\infty - \rho)$ is transformed to a corresponding temperature difference with the aid of equation (1). Since the thermal conditions along the wall $x = L$ which bounds the external flow are not of an elementary type, there is no hope of encountering a similarity solution. Therefore, the conservation equations have to be dealt with in their partial-differential equation form.

To attain the simplest dimensionless form of the conservation equations for the external flow, the following change of variables is made

$$\hat{U} = (uL/v)/Gr^{1/4}, \quad \hat{V} = (vL/v)/Gr^{1/2}, \\ \theta = (T - T_\infty)/(T_h - T_\infty) \quad (10)$$

$$\chi = (x'/L)Gr^{1/4}, \quad x' = x - L, \quad Y = y/L. \quad (11)$$

The different scaling of u and v and of x and y is consistent with the known characteristics of natural-convection boundary-layer flows. Note also that x and y respectively denote the transverse and streamwise coordinates, in contrast to the usual designations.

With these, the dimensionless conservation equations for the boundary layer are

$$\frac{\partial \hat{U}}{\partial \chi} + \frac{\partial \hat{V}}{\partial Y} = 0 \quad (12)$$

$$\hat{U} \frac{\partial \hat{U}}{\partial \chi} + \hat{V} \frac{\partial \hat{U}}{\partial Y} = \theta + \frac{\partial^2 \hat{U}}{\partial \chi^2} \quad (13)$$

$$\hat{U} \frac{\partial \theta}{\partial \chi} + \hat{V} \frac{\partial \theta}{\partial Y} = \frac{1}{Pr} \frac{\partial^2 \theta}{\partial \chi^2}. \quad (14)$$

In these equations, only one parameter, the Prandtl number, appears.

In the transformations that were employed for the internal and external problems, the same thermophysical properties were employed for both. This approach was adopted to avoid involvement with

an excessive number of prescribable parameters. It may also be noted that aside from Y and θ , different transformations were employed for the internal and external problems. This does not cause any difficulties, since, as will be shown, it is only Y and θ that are involved in the continuity relations that link the internal and external problems. The internal transformation is precisely that which would have been employed for the case of pure internal flow (no coupling to an external flow), while the external transformation is that which would have been used had the external flow acted alone.

Attention may now be turned to the boundary and continuity conditions. The velocity boundary conditions are those that are commonly employed

$$U = V = 0, \quad \hat{U} = \hat{V} = 0 \text{ on solid boundaries} \quad (15)$$

$$\hat{V} \rightarrow 0 \text{ as } \chi \rightarrow \infty. \quad (16)$$

For the temperature, the conditions

$$\theta = 1 \quad \text{and} \quad \frac{\partial \theta}{\partial Y} = 0 \quad (17)$$

are respectively appropriate for the left-hand boundary and for the top and bottom boundaries of the enclosure, while for the external flow

$$\theta \rightarrow 0 \text{ as } \chi \rightarrow \infty. \quad (18)$$

The remaining conditions are those which deal with the temperature and heat flux at the boundary $x = L$ which separates the internal and external flows (i.e. the right-hand boundary of the enclosure). There are various models which can be considered for the heat transfer processes in the wall that separates the flows. The simplest model is that in which both the thermal resistance across the thickness of the wall and the net conduction in the streamwise direction are negligible. For that case, which is the one to be considered here, both the temperature and the heat flux are continuous across the thickness of the wall.

The manner in which the continuity conditions are employed depends on the specifics of the method used to solve the conjugate problem. The solution methodology will now be described.

Solution methodology

In view of the complexity of the conjugate problem, a numerical solution is mandatory. The general approach is to work separately and *successively* with the two flows, feeding thermal information from one flow to the other across the common boundary $x = L$. Thus, for fixed values of the parameters, the solution procedure begins with the internal flow, then goes to the external flow, then returns to the internal flow, and so on until a converged solution is obtained. The key feature in the procedure is the method used to transfer information between the two flows, as will now be described.

It has been our experience that in conjugate problems, more rapid convergence of an iterative

solution scheme is achieved if, whenever possible, thermal information is transferred via the heat transfer coefficient than via the temperature or the heat flux. This is because at any stage of an iterative scheme, the transfer coefficient is usually closer to its converged value than are other quantities.

With this in mind, the thermal boundary condition at $x = L$ for the internal flow was written as

$$-k \frac{\partial T}{\partial x} = h(T - T_\infty), \quad x = L \quad (19)$$

where h is the local heat transfer coefficient for the external natural convection boundary layer flow adjacent to $x = L$. The numerical values of h needed in implementing equation (19) are not actually known until the solution procedure has converged. However, since the procedure is an iterative one, provisional values of h can be used at each stage of the iteration, and these provisional values are successively refined as the solution converges.

With regard to the thermal boundary condition at $x' = 0$ (i.e. $x = L$) for the external flow, initial consideration was given to a representation analogous to equation (19), that is

$$-k \frac{\partial T}{\partial x'} = h_{\text{int}}(T_\infty - T), \quad x' = 0 \quad (20)$$

where h_{int} represents the local coefficient at $x = L$ for the internal flow. The subscript symbol ? conveys the uncertainty that prevails about the rational choice of a reference temperature on which to base the definition of the local coefficient. We were unable to identify a simple reference temperature which truly participates in driving the internal heat transfer at $x = L$. Because of this, equation (20) was not employed as a boundary condition for the external flow. Rather, at each stage of the iteration, the external flow was solved with a given surface temperature distribution at $x' = 0$. The temperature distribution, θ vs Y , was taken from the immediately preceding internal flow computation.

Taking the above paragraphs into account, a possible scenario for the numerical solution of the conjugate problem might proceed as follows. First, the parameters Gr and Pr are chosen. Then, for any selected uniform wall temperature at $x' = 0$, the external natural-convection boundary layer is solved, yielding the distribution of the heat transfer coefficient along the wall. Next, attention is shifted to the internal problem, and the just-determined external heat transfer coefficients are used as input to the boundary condition (19). The internal problem is then solved, and this solution yields the temperature distribution along $x = L$. That temperature distribution serves as the wall boundary condition for the external boundary layer, and the corresponding solution provides an updated distribution of the heat transfer coefficient. These coefficients are transmitted to equation (19), and the internal problem is re-solved. This procedure may be continued until convergence is achieved.

The just-discussed procedure, while plausible, is not the one that was actually employed to solve the problem. The reason for its not being used can be explained by noting that the natural-convection heat transfer coefficient for boundary-layer flow should respond to the local wall-to-ambient temperature difference as well as to the streamwise distance from the leading edge. In the aforementioned scheme, the h values, as used in equation (19) and as perceived by the internal flow solution, are a given function of position at each stage of the iteration (the function of position changes from cycle to cycle). However, as the internal solution updates the wall-temperature distribution along $x = L$, h does not respond promptly. Indeed, the effect of the updated wall temperature on h is not felt by the internal solution until the next cycle of the iteration. It is this lag that prompted the use of another approach, which will now be described.

To begin, it may be noted that for natural convection about a vertical plate with a uniform wall temperature T_w , the local heat transfer coefficient for $Pr = 0.7$ is

$$h = (0.3532k/y)[g\beta(T_w - T_\infty)y^3/\nu^2]^{1/4}. \quad (21)$$

Suppose that for a plate with a variable wall temperature T_{wy} , equation (21) were to be applied locally (i.e. replace T_w by T_{wy}) to predict $h(y)$. If such predictions were then compared with the actual $h(y)$ values obtained from a solution of the boundary layer equations, deviations would be encountered. Let $\Omega(y)$ denote the ratio of the actual $h(y)$ to that predicted by equation (21). Then, error-free predictions would be obtained by modifying equation (21) to read

$$h = (0.3532k\Omega(y)/y)[g\beta(T_{wy} - T_\infty)y^3/\nu^2]^{1/4}. \quad (22)$$

Equation (22) is the h formula which was used as input to the boundary condition (19), with the provision that T_{wy} be treated as an unknown as the computations for the internal problem are being performed. This enables the updating of the wall-temperature distribution which occurs during the internal solution to have an immediate effect on the h distribution. The substitution of (22) into (19) and the introduction of dimensionless variables yields

$$(-\partial\theta/\partial X)/Gr^{1/4} = 0.3532\Omega(Y)\theta^{5/4}/Y^{1/4}, \quad X = 1 \quad (23)$$

where Gr is a prescribed constant.

Now, with equation (23) in hand, the steps of solution will be described. As before, values of the parameters Gr and Pr are selected and fixed. Attention is first focused on the internal problem, which is solved subject to $\Omega(Y) = 1$ in equation (23). The resulting $\theta(Y)$ at $X = 1$ becomes the wall boundary condition for the external problem, the solution to which yields a distribution of $\Omega(Y)$ as discussed in the text following equation (21). In particular, if $\partial\theta/\partial\chi$ is the local derivative at the wall which results from the boundary-layer solution, $\Omega(Y)$ is evaluated as

$$\Omega(Y) = (-\partial\theta/\partial\chi)Y^{1/4}/0.3532\theta^{5/4}, \quad \chi = 0. \quad (24)$$

The thus-determined $\Omega(Y)$ are fed to equation (23), and the internal problem is solved anew. The wall temperatures at $X = 1$ from that solution are inputted to the boundary-layer problem, whose solution yields an updated set of $\Omega(Y)$ via equation (24). This procedure is continued until convergence.

Now that the general pattern of the solution methodology has been established, attention will be turned to certain relevant details. Numerical solutions of the boundary layer problem were obtained by employing the Patankar–Spalding method [5]. This is an implicit finite-difference scheme, a special feature of which is that as the boundary-layer thickness varies, the grid automatically follows the variation. To ensure high accuracy consistent with reasonable execution time, a step size study was performed prior to the initiation of the main calculations, with the available similarity solution for uniform wall temperature used as a standard. The final grid pattern encompassed 160 points in the cross-stream direction and slightly less than 5000 points in the streamwise direction. This large number of points ($\sim 800\,000$) was easily accommodated because of the marching nature of the solution in the streamwise direction. In particular, to obtain the solution at any streamwise station, it is only necessary to know the values of the dependent variables at the station immediately upstream.

As explained in the Introduction, the internal-flow problem requires a solution scheme that is basically different from that used for the boundary layer. The scheme employed here is that of Patankar [6]. It is iterative in nature, beginning with guessed values for U , V , P and θ and then refining these values until convergence. At this point, it is important to draw a sharp distinction between the two types of iterations that were required in solving the conjugate problem. One type is the cyclic and successive involvement with the internal and external problems, passing from one to the other as described earlier. The other iterations are those required to solve the internal flow problem at each stage of the aforementioned cyclic procedure.

A 30×30 grid was employed to solve the internal problem. The deployment of the grid was tailored to the specifics of the velocity field for each Grashof number. The tailoring was performed on the basis of preliminary computer runs for 10^3 , 10^4 , ..., and 10^7 for the standard enclosure problem ($\theta = 1$ and $\theta = 0$, respectively at the left- and right-hand boundaries). From these solutions, velocity and temperature field graphs were prepared and, with these, the grid points were positioned so as to resolve all of the main features of the flow. This grid deployment was then used for all of the final computer runs.

Convergence of the iterative scheme for the internal flow problem was attained without difficulty. The initial guessed values were $U = V = P = 0$ and $\theta = 1$. Both U and V were underrelaxed, with an underrelaxation factor of 0.5 for all Gr , except for $Gr = 10^7$ where a factor of 0.2 was used for V . The temperature θ was not underrelaxed for $Gr = 10^3$ and

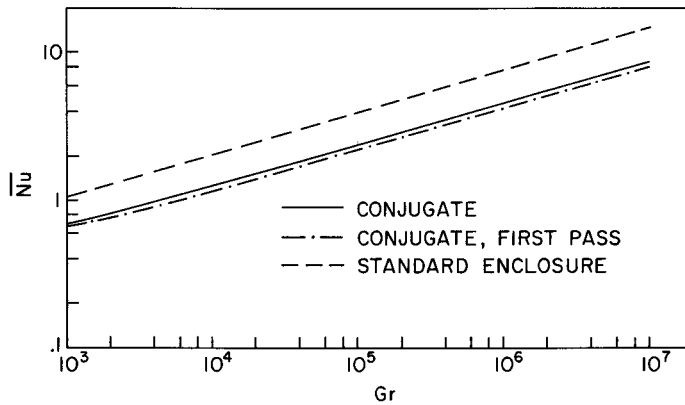


FIG. 2. Average Nusselt numbers.

10^4 , while factors of 0.8, 0.5 and 0.5 were employed for $Gr = 10^5$, 10^6 and 10^7 .

As noted in the Introduction, a set of solutions for the standard enclosure problem was obtained for comparison with those for the conjugate problem. For the standard problem, only the internal flow need be solved, and the Patankar method [6] was employed for the purpose. The starting values for the iterative solution were as stated in the preceding paragraph, except that θ was selected to vary linearly between one and zero between the two vertical walls. The relaxation factors used in these solutions were identical to those used in the conjugate problem.

As a validation of the solution method, the present heat transfer results for the standard enclosure problem were compared with those of McGregor and Emery [7]. The Grashof number range of McGregor and Emery extended up to about 2×10^5 rather than to the present 10^7 . Within our ability to read the graphical presentation of McGregor and Emery, it appears that agreement at the one per cent level prevails.

RESULTS AND DISCUSSION

The presentation of results begins with the average Nusselt number for the conjugate problem as a whole, spanning both the internal and external flows. This is followed by the local heat transfer results for the thermally active walls. Temperature distributions are then presented for the wall which separates the two flows and for the adiabatic walls of the enclosure. Local heat transfer coefficients for the external natural convection flow will be conveyed in terms of the Ω parameter that was introduced in equation (22). The presentation concludes with flow patterns for representative cases displayed via streamline maps.

Heat transfer

The overall rate of heat transfer Q passing across the

enclosure into the ambient fluid can be evaluated by integrating the local heat flux along either of the thermally active walls of the enclosure or along the bounding surface of the external flow. All of these integrations yield identical results. If an average Nusselt number \overline{Nu} is defined as

$$\overline{Nu} = (Q/L(T_h - T_\infty))(L/k) \quad (25)$$

it follows that, for instance, at the right-hand wall of the enclosure

$$\overline{Nu} = \int_0^1 \frac{-\partial\theta}{\partial X} dY \quad (26)$$

The average Nusselt number results for the conjugate problem are plotted as a solid line in Fig. 2 as a function of the Grashof number. There are, in addition, two other lines in Fig. 2. The dashed line portrays the \overline{Nu} results for the standard enclosure problem with uniform temperatures T_h and T_c on the respective vertical walls of the enclosure [Fig. 1(a)]. In this connection, it is important to note the different definitions of \overline{Nu} and Gr for the standard enclosure relative to those for the conjugate problem. The difference is that T_∞ is replaced by the cold-wall temperature T_c , so that, for the standard enclosure

$$\overline{Nu} = (Q/L(T_h - T_c))(L/k),$$

$$Gr = g\beta(T_h - T_c)L^3/\nu^2. \quad (27)$$

The third of the lines in Fig. 2 represents a simplified computational model for the conjugate problem. As noted earlier, the conjugate problem was solved by cyclically passing back and forth between the internal and external flows until convergence was attained. An approximate solution can be obtained for the internal flow which avoids these cyclic visitations and which is, therefore, at the same level of computational involvement as the standard enclosure problem. The idea is to carry out only the first part of the first round of the cyclic process. This amounts to solving the

internal flow problem using equation (23) with $\Omega = 1$ as the boundary condition at $X = 1$, but with no visitation of the boundary-layer problem. This approach, albeit approximate, yields a solution of the conjugate problem without conjugate computations.

Examination of Fig. 2 reveals the expected trend whereby the average Nusselt number increases monotonically with the Grashof number. The dependence of \overline{Nu} on Gr , while not precisely linear on logarithmic coordinates, is very nearly linear over most of the range. For the conjugate problem, the results can be represented to within $\pm 1.5\%$ for $Gr \geq 10^4$ by the power law

$$\overline{Nu} = 0.0907Gr^{0.285}. \tag{28}$$

For $Gr < 10^4$, there is a departure from the (logarithmically) linear behavior indicated by equation (28), so that at $Gr = 10^3$ the \overline{Nu} of (28) is about 7% low compared with the value from the computer solutions.

The existence of a power-law representation for the heat transfer in a conjugate convection problem is, in itself, worthy of note. Although the two participating flows individually yield power-law representations at sufficiently high Grashof numbers, this is no guarantee that the conjugate problem will also yield a power law. In the present instance, perhaps it is the fact that the power-law exponents for the component flows are more or less the same (in the 0.25–0.30 range) that establishes the power law for the conjugate problem.

The heat transfer results from the first-pass solutions for the conjugate problem lie slightly below those for the fully converged solutions, the maximum deviations

being about 8%. In view of the computational simplifications afforded by the first-pass solution, an inaccuracy of 8% may be regarded as tolerable.

The results for the standard enclosure problem are well represented (albeit not precisely) by a power law which applies over the entire range investigated

$$\overline{Nu} = 0.141Gr^{0.29}. \tag{29}$$

Equation (29) represents the computed results to $\pm 1.8\%$. The exponent in equation (29) is very nearly the same as that in equation (28), and a common exponent might well have been used.

To compare the results for the conjugate problem with those for the standard enclosure requires that some specification be made of the relative magnitudes of $(T_h - T_\infty)$ and $(T_h - T_c)$, since these temperature differences appear in the respective Nusselt and Grashof numbers. For the case in which these temperature differences are the same, the Nusselt numbers for the conjugate problem are about 60% of those for the standard enclosure for $Gr \geq 10^4$, with somewhat smaller deviations at lower Grashof numbers. The lower Nu values for the conjugate problem can be attributed to the thermal resistance of the external flow. It is, however, quite remarkable that the deviations are so uniform over so large a range of Grashof numbers.

Attention will now be turned to the local heat transfer results for the thermally active walls. These results are shown in Figs. 3 and 4 for the left-hand wall (the heated wall) and the right-hand wall (the cooled wall), respectively. Each figure is subdivided into two panels [(a) and (b)]. The (a) panel conveys the

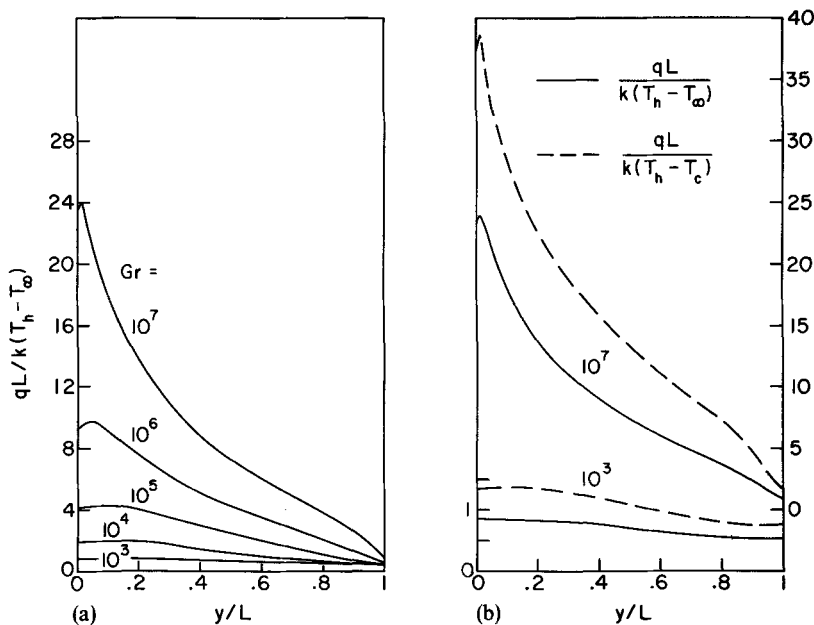


FIG. 3. Local heat flux distributions for the heated isothermal wall.

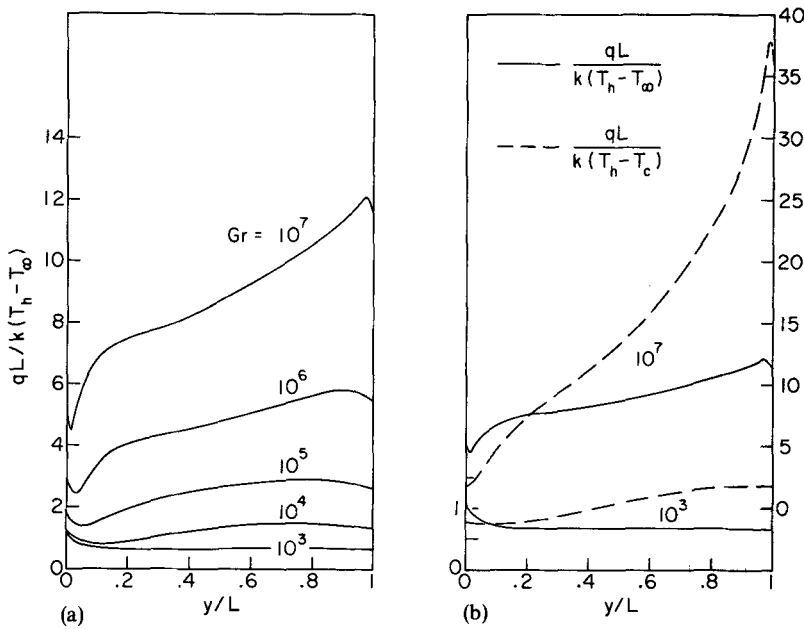


FIG. 4. Local heat flux distributions for the convectively cooled wall.

distributions of the local heat flux for the conjugate problem while the (b) panel shows comparisons between results for the conjugate problem and the standard enclosure.

Turning first to Fig. 3(a), it may be noted that the fluid flow is in the direction of increasing y . Thus, as the fluid passes upward along the hot wall, its temperature increases and the boundary layer thickens, with a resultant decrease of the local heat flux as portrayed in the figure. The sharpness of the decrease is most marked at the higher Grashof numbers. At lower Grashof numbers, convection wanes and the distribution becomes more uniform as conduction takes over. The shapes of the high- Gr distributions in the neighborhood of $y = 0$ suggest the presence of a low-velocity region (perhaps a sluggish recirculation zone) in the corner at the base of the wall.

In Fig. 3(b), the heat flux distributions for the conjugate problem are compared with those for the standard enclosure for $Gr = 10^3$ and 10^7 . The distribution curves for the two problems are seen to be remarkably similar in shape, suggesting similarity in the flow fields adjacent to the hot wall. For quantitative comparisons of heat flux magnitudes, it is once again necessary to specify the relative magnitudes of $(T_h - T_\infty)$ and $(T_h - T_c)$. For the case where these temperature differences are the same, the heat fluxes for the standard enclosure exceed those for the conjugate problem, the percentage deviations being similar to that for the overall heat transfer (i.e. the average Nusselt number).

In assessing the local heat flux distributions of Fig. 4 for the cooled wall (i.e., the right-hand wall), it is

relevant to note that the internal flow moves downward along the wall, i.e. from $y/L = 1$ to $y/L = 0$. Thus, it might be expected that the heat flux would decrease as y/L decreases from 1 to 0. This trend is, in general, in evidence in Fig. 4(a), which conveys the results for the conjugate problem. However, it is interesting to note that these decreases of q along the flow direction are substantially smaller than those of Fig. 3 for the hot wall. The reason for the greater uniformity of q on the cooled wall is the counterflow nature of the heat transfer process at that wall. As indicated in Fig. 1(b), the downward internal flow transfers heat to the upward external flow. The tendency for q to take on a local maximum at $y = 0$ can be attributed to the very high values of the external heat transfer coefficient in that region.

In Fig. 4(b), comparisons are made between the cooled-wall heat flux distributions for the conjugate problem and the standard enclosure problem. These comparisons show that the heat flux for the standard enclosure is much more nonuniform than that for the conjugate problem. This greater nonuniformity for the standard problem is due to the absence of the aforementioned counterflow effect which prevails in the conjugate problem.

Wall temperature distributions

The distribution of the temperature along the wall which separates the internal and external flows is presented in Fig. 5(a) with the Grashof number as the curve parameter. Comparisons of the results from the first-pass solutions with those from the fully converged solutions are shown in Fig. 5(b).

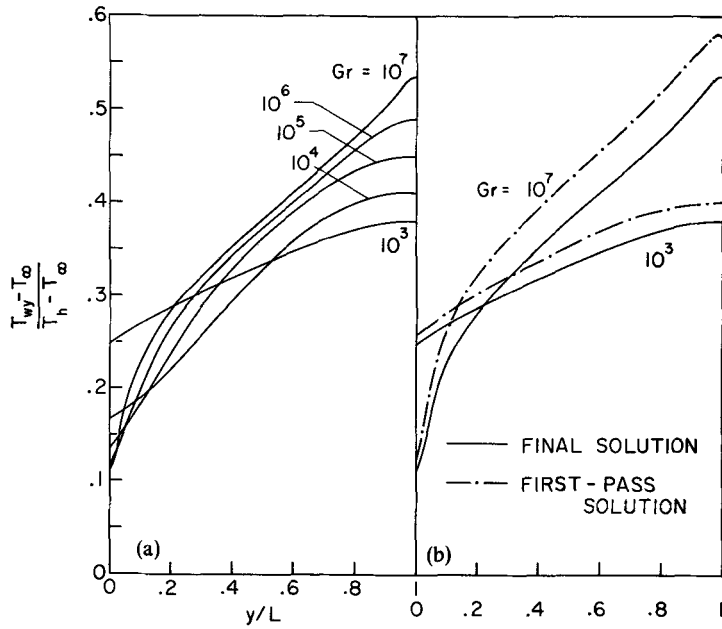


FIG. 5. Temperature distributions along the wall which separates the internal and external flows.

In interpreting the results of the figure, it should be noted that the direction of the internal flow is from $y/L = 1$ to 0 and that the internal flow loses heat to the external flow as it passes along the wall. The decrease of the wall temperature with decreasing y/L is, therefore, entirely plausible. Also plausible are the progressively higher values of the wall temperature at $y/L = 1$ which accompany an increase in the Grashof

number. The temperature elevation occurs because the higher Grashof number flow is more effective in carrying higher temperature fluid from the hot wall across to the convectively cooled wall.

The wall temperature is seen to be increasingly more nonuniform as the Grashof number increases. The relative uniformity of the temperature at the lower Grashof numbers is due to the waning of convection

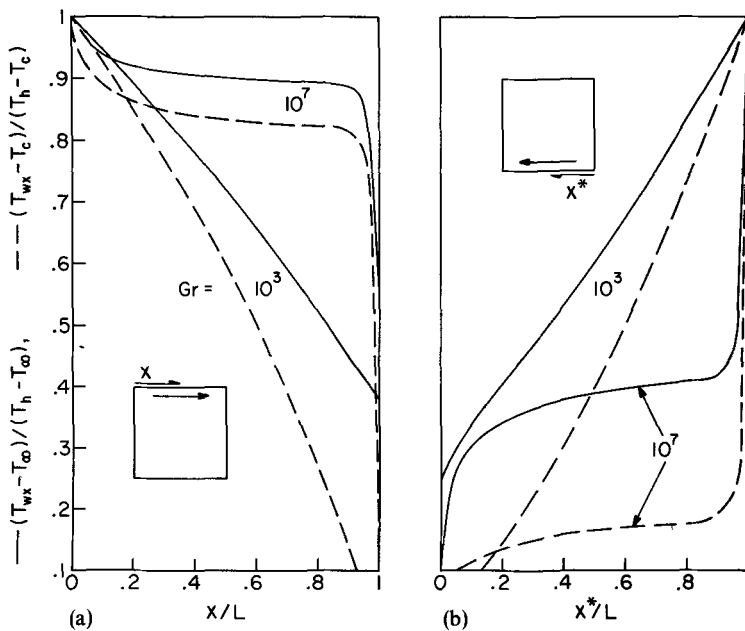


FIG. 6. Representative temperature distributions along the adiabatic walls of the enclosure. (a) Upper wall; (b) lower wall.

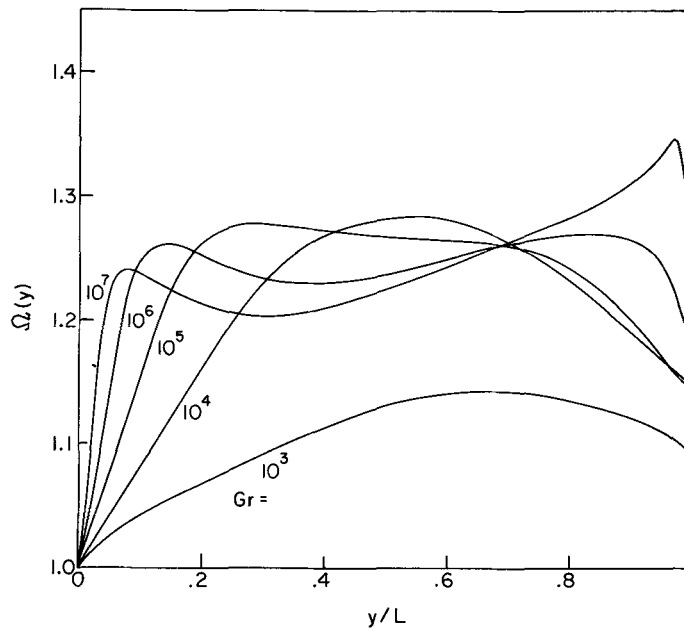


FIG. 7. Distributions of Ω to be used in the Nusselt number representation, equation (30), for the external natural convection flow.

and the growing importance of heat conduction.

Figure 5(b) shows that the first-pass solution yields temperature distributions which are similar in shape to those of the converged solution. Generally, the first-pass solution tends to overestimate the wall temperature, but the errors appear to be tolerable.

Representative temperature distributions along the adiabatic walls of the enclosure are shown in Fig. 6(a), which pertains to the upper wall, while Fig. 6(b) pertains to the lower wall. To facilitate interpretation of the results, the coordinate directions have been taken along the respective directions of fluid flow as indicated in the inset of each part of the figure. Results are provided both for the conjugate problem and for the standard enclosure problem (solid and dashed lines, respectively).

In considering Fig. 6(a), note may be taken of the significant Grashof-number-related differences in the temperature distribution along the upper wall. At high Grashof numbers, the vigorous recirculating flow blankets the upper wall with hot fluid (i.e. fluid previously heated at the left-hand wall of the enclosure). Consequently, high temperatures are in evidence along the upper wall. On the other hand, at relatively low values of Gr , the convection is relatively weak and conduction forces a more or less linear temperature variation across the enclosure. The qualitative trends are similar for both the conjugate problem and the standard enclosure problem.

The just-cited factors which operate to establish the temperature distributions along the upper wall are also operative along the lower wall, as can be seen in Fig. 6(b). The orientations of the curves in the two

parts of the figure are just opposite because of the opposite fluid-flow directions along the upper and lower walls. The quantitative deviations between the high- Gr solid and dashed curves in the right-hand panel are greater than those in the left-hand panel. This is because the thermal conditions along the right-hand wall are different in the conjugate and standard enclosure problems.

Nusselt numbers for the external flow

From the converged solutions for the conjugate problem, the local heat transfer coefficients and corresponding Nusselt numbers for the external natural convection flow have been deduced. These results may be phrased in the form

$$hy/k = 0.3532\Omega[g\beta(T_{wy} - T_{\infty})y^3/\nu^2]^{1/4} \quad (30)$$

where $\Omega = \Omega(y)$ is presented in Fig. 7 and T_{wy} is the local wall temperature at y .

With $\Omega = 1$, equation (30) depicts the application of the h formula for uniform wall temperature to a situation where the wall temperature varies along the flow direction. The fact that $\Omega \neq 1$ (Fig. 7) demonstrates that direct local application of the isothermal wall formula to a nonisothermal wall is not strictly valid. In a sense, Ω plays the role of a correction factor which redresses any errors made by local application of the h formula.

Figure 7 shows that the distribution of Ω along the wall evolves with increasing Grashof number. At the lowest Grashof number investigated, Ω varies smoothly with y and departs only moderately from unity. As Gr increases, the level of Ω tends at first to

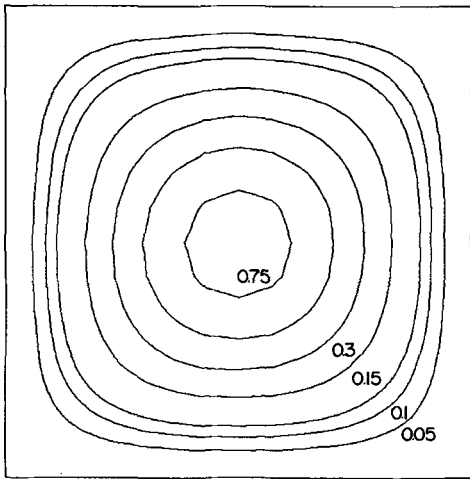


FIG. 8. Streamline pattern for $Gr = 10^3$. The curve parameter is ψ/v .

increase, but further increases in Gr are mainly instrumental in altering the shape of the Ω distribution. For Grashof numbers greater than 10^3 , the Ω values are, for the most part, in the range 1.2–1.3. The fact that $\Omega > 1$ is consistent with the increase of T_{wy} in the direction of the boundary-layer flow.

Flow patterns

The qualitative nature of the fluid flow in the enclosure can be effectively visualized with the aid of streamline maps. Representative streamline maps based on the solutions of the conjugate problem are presented in Figs. 8 and 9. The figures correspond to Grashof numbers of 10^3 and 10^7 , which are, respectively, the smallest and largest values that were investigated. The numerical labels that are used to identify the contour lines in each figure correspond to

the dimensionless streamfunction ψ/v .

Comparison of Figs. 8 and 9 reveals numerous Grashof-number-related differences in the flow fields. At low Grashof numbers, there is an all-encompassing symmetry such that the flow field adjacent to the adiabatic walls (the horizontal walls) is virtually identical to that adjacent to the thermally active walls (the vertical walls). On the other hand, at high Grashof numbers, the streamlines are crowded together next to the active walls while they are widely spaced adjacent to the adiabatic walls. The crowding of the streamlines is indicative of a boundary-layer-type flow along the active walls. Figure 8 shows that a Grashof number of 10^3 is too low to produce boundary layer flows.

Aside from the aforementioned differences in the shapes of the streamlines, there are also marked differences in the magnitudes of the streamfunction for the two Grashof numbers. The streamfunction values of $Gr = 10^7$ are about 40 times those for $Gr = 10^3$. This means that the buoyancy-induced mass flows for the two cases bear that ratio to each other. Furthermore, since $u = \partial\psi/\partial y$ and $v = -\partial\psi/\partial x$, it is clear that the velocities are markedly larger at higher Grashof numbers. In particular, the solutions show that U_{\max} for $Gr = 10^7$ is about 100 times the U_{\max} value for $Gr = 10^3$; the corresponding ratio of the V_{\max} values is about 250.

In the streamline map for $Gr = 10^7$, modest asymmetries of the flow with respect to the two active walls are in evidence. These asymmetries are due to the different thermal boundary conditions at the two walls.

The streamline maps of Figs. 8 and 9 are qualitatively similar to those for the standard enclosure at the same values of the Grashof number. Quantitative comparisons require specification of the relationship between the temperature differences $(T_h - T_\infty)$ and $(T_h - T_c)$ which appear in the respective Grashof number definitions.

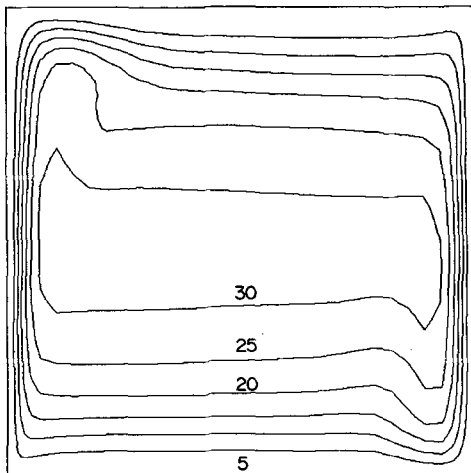


FIG. 9. Streamline pattern for $Gr = 10^7$. The curve parameter is ψ/v .

CONCLUDING REMARKS

Solutions have been obtained here for a conjugate natural convection problem encompassing a buoyancy-driven recirculating flow in an enclosure and an external natural-convection boundary-layer flow along one of the walls of the enclosure. In addition to the complete numerical solutions, a set of approximate solutions were carried out which avoids computational involvement with the boundary-layer flow and focuses all numerical activity in the enclosure. To provide perspective for the results of the conjugate problem, numerical solutions were also obtained for the standard enclosure problem in which the two vertical walls have prescribed uniform temperatures while the two horizontal walls are adiabatic.

The solutions spanned the range of Grashof number between 10^3 and 10^7 , with the Prandtl number equal to 0.7 in all cases. The enclosure geometry was square.

The overall heat transfer characteristics for the

conjugate problem as a whole, encompassing both the internal and external flows, were expressed in terms of the average Nusselt number \overline{Nu} . For $Gr \geq 10^4$, the \overline{Nu} - Gr relationship was well represented (to within $\pm 1.5\%$) by the power law: $\overline{Nu} = 0.0907Gr^{0.285}$. At low Gr , the \overline{Nu} values tend to fall above those given by the power law. The approximate solutions yielded \overline{Nu} values that are slightly lower than those from the complete solutions, with a maximum deviation of about 8%. The \overline{Nu} results for the standard enclosure could also be well represented by a power law $\overline{Nu} = 0.141Gr^{0.29}$ to within $\pm 1.8\%$ over the range $Gr \geq 10^3$. If $(T_h - T_\infty)$ for the conjugate problem were equal to $(T_h - T_c)$ for the standard enclosure, the \overline{Nu} for the former would be about 60% of those for the latter when $Gr \geq 10^4$.

The local heat fluxes at the thermally active walls of the enclosure tend to decrease in the direction in which fluid flows along the respective walls. The extent of the variation is much smaller along the convectively cooled wall than along the isothermal heated wall, reflecting the counterflow nature of the heat exchange between the internal and external flows at the convectively cooled wall. At lower Grashof numbers, the local heat flux distributions tend toward greater uniformity.

At the wall which separates the internal and external flows, the temperature decreases in the direction of the internal flow. This decrease results from the heat loss by the internal flow to the external flow as it passes along the wall. The extent of the temperature variation along the wall increases with increasing Grashof number. The temperatures at the adiabatic walls of the enclosure are strongly affected by the Grashof number. At high Grashof numbers, the relatively vigorous recirculating flow impresses its temperature history on the adiabatic walls, while at low Grashof numbers heat

conduction is the key factor in establishing the temperature at these walls.

The local heat transfer coefficients for the external natural convection are generally higher than those predicted by locally applying the h formula for uniform wall temperature. At the higher Grashof numbers, the deviations are in the 20–30% range.

Streamline maps revealed marked Grashof-number-related differences in the flow pattern within the enclosure. At low Gr , the flow field adjacent to the adiabatic walls is similar to that adjacent to the thermally active walls, and there is no evidence of boundary-layer-type flow. On the other hand, at large Gr , boundary layer flows occur adjacent to the active walls but not along the passive walls.

Acknowledgement—The research reported here was performed under the auspices of the National Science Foundation.

REFERENCES

1. S. Ostrach, Natural convection in enclosures, *Adv. Heat Transfer* **8**, 161–227 (1972).
2. I. P. Jones, A numerical study of natural convection in an air-filled cavity: comparison with experiment, *Num. Heat Transfer* **2**, 193–213 (1979).
3. J. N. Reddy and A. Satake, A comparison of a penalty finite element model with the stream function–vorticity model of natural convection in enclosures, *J. Heat Transfer* **102**, 659–666 (1980).
4. A. Bejan, A synthesis of analytical results for natural convection heat transfer across rectangular enclosures, *Int. J. Heat Mass Transfer* **23**, 723–726 (1980).
5. S. V. Patankar and D. B. Spalding, *Heat and Mass Transfer in Boundary Layers*, 2nd edn. Intertext, London (1970).
6. S. V. Patankar, *Numerical Heat Transfer and Fluid Flow*. Hemisphere Publishing, Washington (1980).
7. R. K. MacGregor and A. F. Emery, Free convection through vertical plane layers—moderate and high Prandtl number fluids, *J. Heat Transfer* **91**, 391–403 (1969).

INTERACTION ENTRE LA CONVECTION NATURELLE DANS UNE CAVITE ET UN ECOULEMENT EXTERNE DE CONVECTION NATURELLE A COUCHE LIMITE

Résumé—On analyse la convection naturelle dans une cavité carrée dont une paroi verticale est refroidie par un écoulement externe de convection naturelle avec couche limite. L'autre paroi verticale est maintenue à température uniforme alors que les parois horizontales sont adiabatiques. Le problème de couplage de convection naturelle interne-externe est résolu numériquement pour des nombres de Grashof entre 10^3 et 10^7 et pour un nombre de Prandtl de 0,7. On obtient aussi des solutions approchées à partir d'un modèle qui évite les calculs de type conjugué. Pour comparaison, on donne les solutions pour le problème classique de convection naturelle dans une cavité avec température imposée sur les parois verticales et avec parois horizontales adiabatiques. Pour les caractéristiques moyennes du transfert thermique, le nombre de Nusselt moyen dépend du nombre de Grashof suivant la loi de puissance $Nu = 0,0907 Gr^{0.285}$ pour $Gr \geq 10^4$. Ce nombre de Nusselt est environ soixante pour cent de celui pour la cavité classique, aux mêmes valeurs du nombre de Grashof. Les variations du flux local le long de la paroi refroidie par convection sont sensiblement plus faibles que celles le long de la surface isotherme chaude, traduisant l'opposition entre les effets thermiques des écoulements interne et externe. De plus les variations de température le long de la paroi refroidie par convection croissent lorsque le nombre de Grashof augmente. Le nombre de Grashof agit sur la distribution de température le long des parois adiabatiques. La carte des lignes de courant montre une petite différence entre les champs d'écoulement adjacents aux parois thermiquement actives et passives aux faibles nombres de Grashof, mais des différences marquées sont visibles aux grands nombres de Grashof. Pour la convection naturelle externe, les coefficients locaux de transfert thermique sont généralement plus grands que ceux obtenus par application de la formule relative au coefficient de transfert sur une plaque isotherme.

WECHSELWIRKUNG ZWISCHEN INNERER FREIER KONVEKTION IN EINEM HOHLRAUM UND EINER EXTERNEN GRENZSCHICHTSTRÖMUNG DURCH FREIE KONVEKTION

Zusammenfassung — Es wird eine Untersuchung durchgeführt über die freie Konvektion in einem quadratischen Hohlraum, von dessen vertikalen Wänden eine durch eine Grenzschichtströmung infolge äußerer freier Konvektion gekühlt wird. Die andere vertikale Wand wird auf gleichförmiger Temperatur gehalten, während die horizontalen Wände adiabat sind. Das auftretende gekoppelte Problem interner und externer freier Konvektion wurde numerisch für Grashof-Zahlen zwischen 10^3 und 10^7 und für eine Prandtl-Zahl von 0,7 gelöst. Näherungslösungen wurden auch mit einem Modell erzielt, welches die gekoppelte Lösung vermeidet. Zu Vergleichszwecken wurde eine Anzahl Lösungen für das Standardproblem freier Konvektion in einem Hohlraum berechnet, das durch vorgegebene gleichförmige Temperaturen an den vertikalen Wänden und adiabate horizontale Wände gekennzeichnet ist. Für den Gesamtwärmedurchgang, der sowohl die interne als auch die externe freie Konvektion umfaßt, zeigt die mittlere Nusselt-Zahl eine Abhängigkeit von der Grashof-Zahl nach einem Potenzgesetz, das bei $Gr \leq 10^4$ durch $\overline{Nu} = 0,0907Gr^{0,285}$ gegeben ist. Diese Nusselt-Zahlen erreichen etwa 60% der Werte für den Standardhohlraum bei üblichen Werten der entsprechenden Grashof-Zahlen. Die örtlichen Variationen des Wärmestroms entlang der konvektiv gekühlten Wand waren merklich kleiner als die an der beheizten isothermen Wand, was im Gegenstromcharakter des Wärmeaustausches zwischen interner und externer Strömung begründet ist. Außerdem nahmen die Temperaturvariationen entlang der konvektiv gekühlten Wand mit zunehmender Grashof-Zahl zu. Die Grashof-Zahl beeinflusste auch maßgebend die Temperaturverteilungen entlang der adiabat Wände. Stromlinienbilder zeigten bei niedrigen Grashof-Zahlen wenig Unterschiede zwischen den Strömungsfeldern nahe den thermisch aktiven und thermisch passiven Wänden, doch wurden markante Unterschiede bei hohen Grashof-Zahlen sichtbar. Bei der externen freien Konvektion waren die örtlichen Wärmeübergangskoeffizienten im allgemeinen größer als die durch örtliche Anwendung der klassischen Formeln für die isotherme Wand berechneten Werte.

ВЗАИМОДЕЙСТВИЕ МЕЖДУ ВНУТРЕННЕЙ ЕСТЕСТВЕННОЙ КОНВЕКЦИЕЙ В ПОЛОСТИ И ВНЕШНИМ ПОГРАНИЧНЫМ СЛОЕМ, ОБРАЗОВАННЫМ ЕСТЕСТВЕННОЙ КОНВЕКЦИЕЙ

Аннотация — Проведён анализ естественной конвекции в квадратной полости, одна из вертикальных стенок которой охлаждается внешним пограничным слоем, образованным естественной конвекцией. На второй вертикальной стенке поддерживается однородная температура, горизонтальные стенки являются адиабатическими. Сопряжённая задача для внутренней и внешней естественной конвекции решена численно для чисел Грасгофа от 10^3 до 10^7 и числа Прандтля 0,7. Приближённые решения были также получены при помощи модели, не связанной с сопряжённой постановкой задачи. С целью сравнения выполнен ряд решений для известной стандартной задачи о естественной конвекции, характеризующейся заданными однородными температурами на вертикальных стенках и адиабатическими горизонтальными стенками. Для описания теплопереноса, включающего как внутренние, так и внешние потоки, предложена степенная зависимость среднего числа Нуссельта от числа Грасгофа: $\overline{Nu} = 0,0907Gr^{0,285}$ для $Gr \geq 10^4$. Данные числа Нуссельта составляют примерно 60% от чисел Нуссельта для стандартной задачи при соответствующих значениях чисел Грасгофа. Было обнаружено, что изменения локального теплового потока вдоль конвективно охлаждаемой стенки значительно меньше, нежели вдоль нагретой изотермической стенки, что обусловлено противоположными направлениями движения внутреннего и внешнего потоков. Кроме того, изменения температуры вдоль конвективно охлаждаемой стенки возрастали с увеличением числа Грасгофа. Число Грасгофа имело решающее влияние также и на распределение температур вдоль адиабатических стенок. Картины линий тока продемонстрировали небольшое различие между полями скоростей, прилегающими к термически активным и термически пассивным стенкам при малых числах Грасгофа, но при больших числах Грасгофа это различие было ярко выраженным. Для случая внешней естественной конвекции местные коэффициенты теплообмена обычно превосходили коэффициенты, предсказываемые классической формулой для коэффициента теплообмена на изотермической пластине.